Monitoring the Spatial Dynamics of Mikania micrantha During the Flowering Season Using Multi-epoch UAV Imagery: A Case Study North of Liyu Lake, Hualien, Taiwan

Yu-Cheng Huang[1], Yi-Ta Hsieh[2], Ping-Hung Chiang[1], Bo-Yi Lin[1], Jan-Chang Chen[1]

[1]National Pingtung University of Science and Technology, 1, Shuefu Road, Neipu, Pingtung 91201, Taiwan, R.O.C. - vito777730@gmail.com
[2]National Ilan University, 1, Sec. 1, Shennong Rd., Yilan City, Yilan County 26047, Taiwan, R.O.C. - ythsieh@niu.edu.tw

Keywords: *Mikania micrantha*, Unmanned Aerial Vehicle, Invasive plant spread, Invasive plant monitoring

Abstract
Mikania micrantha is one of the most aggressive invasive alien plant species in low-elevation landscapes of Taiwan. This study used fixed-wing UAV imagery to monitor its flowering-season distribution in a primary monitoring area north of Liyu Lake, Hualien County, eastern Taiwan. Rather than treating the dataset as a continuous annual time series, the analysis was based on three flowering-season observation epochs acquired on 14 January 2021, 7 December 2021, and 4 January 2024. UAV imagery was collected using an eBee X platform and processed in Pix4Dmapper Pro to generate high-resolution RGB orthomosaics with an average ground sampling distance of 3.08 cm/pixel. *M. micrantha* patches were delineated through manual image interpretation, and kernel density estimation (KDE) was applied to evaluate changes in spatial concentration and hotspot distribution. The interpreted infestation area decreased from 2,094.74 m² in the first epoch to 1,361.94 m² in the second, then increased to 1,799.09 m² in the third. KDE results showed a similar pattern, with persistent core infestation zones and renewed expansion in surrounding areas, including a new hotspot in the southeastern part of the monitoring area. These findings demonstrate the practical value of UAV-based monitoring for adaptive invasive plant management.

1. Introduction

1.1 Background and Motivation

Biological invasions have become one of the major drivers of ecosystem degradation and biodiversity loss worldwide (Meiners et al., 2001; Seebens et al., 2018). Although the impacts of invasive plant species are sometimes less immediate than those caused by invasive pathogens, herbivores, or predators, their long-term effects on native vegetation, habitat structure, and ecosystem functioning can be profound. Invasive alien plants may alter species composition, suppress native regeneration, reduce habitat quality, and generate substantial losses in agriculture and forestry. As the introduction and establishment of alien plant species continue to increase, effective detection, monitoring, and management have become increasingly important for preventing further ecological and economic damage (Pyšek et al., 2004; Tye, 2006).

M. micrantha Kunth is among the most aggressive invasive alien plant species in tropical and subtropical Asia and has become widely established in low-elevation areas of Taiwan (Huang et al., 2003). This perennial climbing vine is characterized by rapid twining growth, vigorous lateral expansion, and strong reproductive capacity. It readily covers shrubs, tree crowns, and cultivated vegetation, thereby reducing light interception by host plants and often causing decline or mortality. In addition to prolific seed production, the species can also regenerate from stem fragments, which gives it a strong capacity for reinvasion even after apparent removal or suppression. As a result, *M. micrantha* has caused persistent ecological disturbance and agricultural losses in many lowland landscapes of eastern Taiwan, especially in disturbed forest edges, abandoned farmlands, plantation margins, and other open or semi-open environments.

Because of its rapid spread and strong reinvasion potential, understanding the spatial distribution of *M. micrantha* is essential for improving management efficiency and prioritizing control efforts (Wei, 2003). Spatial monitoring not only helps identify current infestation hotspots, but also provides critical information on whether previously treated areas remain stable, recover, or become reinvaded. Such information is particularly valuable for adaptive management, because effective control of invasive plants depends not only on initial removal, but also on the continuous evaluation of follow-up outcomes and the timely identification of new outbreak zones (Chen, 2017).

In recent years, unmanned aerial vehicle (UAV) remote sensing has emerged as an efficient tool for vegetation monitoring because of its high spatial resolution, operational flexibility, and ability to provide site-specific imagery within short time intervals (Feng et al., 2021). Compared with conventional field surveys, UAV imagery can rapidly capture fine-scale spatial patterns over heterogeneous terrain and can support repeated observations for management-oriented monitoring. In the context of invasive plant detection, UAV-based approaches are particularly useful when the target species exhibits distinct canopy structure, flowering characteristics, or seasonal color changes that can be identified in aerial imagery. During the flowering and senescence period, *M. micrantha* often presents bright green to whitish-green inflorescences and, later, grayish-white or brownish patches, which make it visually distinguishable from adjacent vegetation in high-resolution RGB orthomosaics.

Although recent studies have increasingly applied automated or semi-automated image classification methods to invasive plant mapping, practical monitoring programs often still face constraints related to sensor availability, annotation cost, variable environmental conditions, and the need for rapid interpretation in support of field management. Under such circumstances, a carefully designed manual interpretation workflow based on high-resolution UAV imagery remains a useful and operationally feasible approach, especially for establishing reliable reference data and documenting local invasion patterns. In management-oriented applications, the value of UAV monitoring lies not only in the production of distribution maps, but also in its ability to reveal persistent hotspots, peripheral spread, and possible reinvasion pathways that may inform subsequent control planning.

Against this background, this study focused on a primary monitoring area located north of Liyu Lake in Shoufeng Township, Hualien County, Taiwan. Fixed-wing UAV imagery acquired during the flowering season was used to investigate the spatial distribution of *M. micrantha* at three observation epochs: 14 January 2021, 7 December 2021, and 4 January 2024. Rather than treating these observations as a continuous annual time series, this study interprets them as three flowering-season observation epochs that allow comparison of infestation extent, spatial concentration, and hotspot persistence across unevenly spaced observations. By integrating UAV image interpretation, field verification, and kernel density analysis, this study aims to provide a practical spatial basis for long-term monitoring and adaptive management of *M. micrantha* in the Liyu Lake region.

1.2 Research Objectives

Based on the above motivation, this study employed UAV imagery interpretation and field verification to examine the flowering-season distribution of *M. micrantha* in the monitoring area north of Liyu Lake at three observation epochs. The study specifically aimed to compare differences in areal extent and spatial concentration among the three epochs and to identify persistent infestation hotspots that may indicate continued reinvasion risk or insufficient suppression. The objectives of this study were as follows:

1. To delineate the flowering-season distribution of *M. micrantha* from UAV imagery at three observation epochs and generate corresponding distribution maps.
2. To compare changes in areal extent and spatial concentration of *M. micrantha* among the three observation epochs.
3. To identify persistent hotspots and potential reinvasion zones as a spatial reference for follow-up monitoring and management planning.

2. Materials and Methods

2.1 Study Area

This study was conducted in a primary monitoring area located approximately 700 m north of Liyu Lake in Shoufeng Township, Hualien County, eastern Taiwan. The site is situated within the northern Huatung Valley and is characterized by a heterogeneous landscape composed of forest edges, grasslands, agricultural land, and semi-open disturbed vegetation. Such environmental conditions provide favorable habitat for the establishment and spread of *M. micrantha*, particularly along ecotones and other open or partially shaded areas where the vine can rapidly expand and overtop surrounding vegetation.

The UAV survey coverage used for image interpretation and subsequent spatial analysis was approximately 0.3487 km² (34.8746 ha). This area served as the spatial extent for orthomosaic generation, manual delineation, and density analysis in this study. The location of the monitoring area is shown in Figure 1.

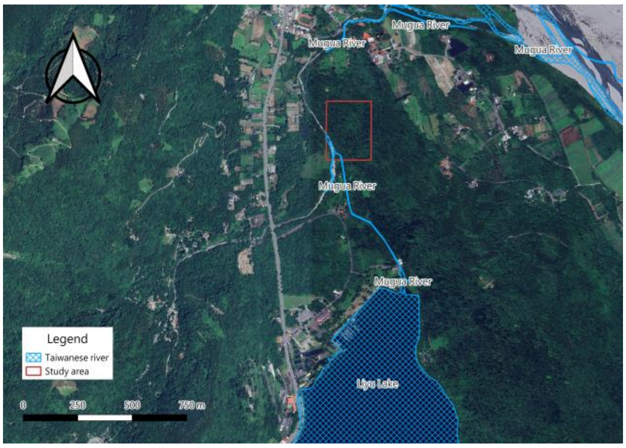

Figure 1. Study Area Map

2.2 Materials

A fixed-wing UAV platform, the eBee X (AgEagle, formerly senseFly), was used for aerial image acquisition in this study. According to the manufacturer’s specifications, the eBee X is a lightweight mapping UAV with a wingspan of 116 cm, an empty weight of 0.8 kg, and a maximum take-off weight of 1.6 kg (Figure 2). The platform supports RTK and PPK georeferencing workflows and is designed for mapping applications with interchangeable imaging payloads, including RGB, multispectral, and thermal sensors. Under appropriate operating conditions, the eBee X can achieve high-precision image geolocation and high-resolution mapping performance suitable for vegetation monitoring. The platform also supports long-endurance missions and is widely used for photogrammetric surveying (Tian et al., 2017).


Figure 2. Sensefly eBee X

In this study, the UAV surveys were conducted during the flowering season of *M. micrantha* at three observation epochs: 14 January 2021, 7 December 2021, and 4 January 2024. According to the available project records, the three missions were carried out using essentially the same flight configuration and processing workflow. The retained Pix4D quality report indicates that the imagery was captured using an RGB camera with the model designation FC6310_8.8_5472x3648. The photogrammetric products were processed in Pix4Dmapper Pro version 3.1.23, and the resulting orthomosaic had an average ground sampling distance (GSD) of 3.08 cm/pixel. The total mapped coverage was 0.3487 km² (34.8746 ha).

https://doi.org/10.5194/isprs-archives-XLIX-B3-2026-121-2026 |

M. micrantha is a perennial invasive climbing vine in the family Asteraceae. It exhibits rapid twining growth, strong lateral spread, and a high capacity for reinvasion through both seed dispersal and vegetative regeneration from stem fragments (Figure 3). During the flowering season, the species displays bright green to whitish-green inflorescences and later develops grayish-white to brownish senescent patches, which are visually distinguishable in high-resolution RGB imagery (Nyamekye et al., 2021). These phenological characteristics formed the basis for aerial image interpretation in this study.

Figure 3. *Mikania micrantha*

2.3 Research Workflow

The overall workflow of this study comprised four main steps: (1) UAV image acquisition during the flowering season of *M. micrantha*; (2) generation of georeferenced RGB orthomosaics; (3) manual interpretation and delineation of *M. micrantha* patches based on phenological and image-structure characteristics; and (4) kernel density estimation (KDE) to evaluate changes in spatial concentration and hotspot distribution across the three observation epochs. The methodological framework is summarized in Figure 4.

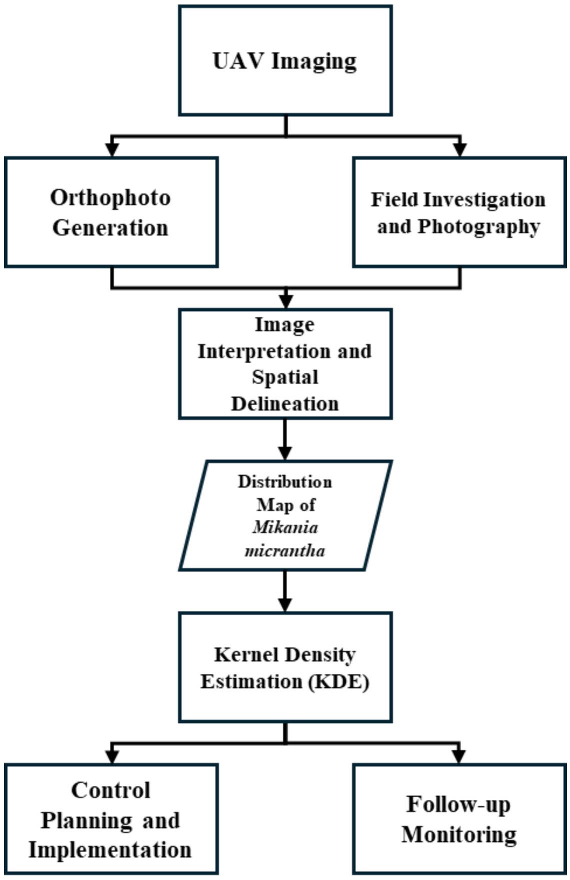

Figure 4. Research Workflow Diagram

2.3.1 UAV Image Acquisition and Orthophoto Generation

Prior to each survey, flight planning was conducted to ensure adequate image quality, consistent scene coverage, and reliable georeferencing for photogrammetric processing. The UAV platform used in this study, the eBee X, supports both RTK and PPK positioning functions, which are intended to improve image geolocation accuracy during or after data acquisition. Although the original mission logs containing parameters such as flight altitude, forward overlap, side overlap, and flight speed were not fully retained, the three survey missions were performed using essentially the same acquisition settings according to the available project records.

The retained quality report for the processed UAV imagery indicates that the imagery was acquired using an RGB camera identified as FC6310_8.8_5472x3648. A total of 381 images were imported into the project, of which 339 images were successfully calibrated, corresponding to 88% of the dataset. All 381 images were geolocated, and the dataset was processed in four image blocks. The resulting orthomosaic had an average GSD of 3.08 cm/pixel, while the DSM and orthomosaic output resolution was set to 1 × GSD, corresponding to 3.09 cm/pixel. The total area covered by the processed imagery was 0.3487 km² (34.8746 ha). The median number of keypoints per image was 78,747, and the median number of matches per calibrated image was 16,966. The bundle block adjustment yielded 5,724,724 2D keypoint observations and 2,352,020 3D points, with a mean reprojection error of 0.146 pixels, indicating generally stable photogrammetric reconstruction quality.

Georeferencing was performed without 3D ground control points (GCPs), as indicated in the quality report. The project used WGS84 (egm96) as the image coordinate system and TWD97 / TM2 zone 121 (egm2008) as the output coordinate system. The mean absolute positional uncertainty of camera positions was reported as 1.132 m in X, 1.146 m in Y, and 2.423 m in Z, while the RMS geolocation error of image positions was 0.334 m in X, 0.444 m in Y, and 2.149 m in Z. Relative camera position uncertainties were substantially smaller, with mean values of 0.080 m, 0.090 m, and 0.102 m for X, Y, and Z, respectively. These values suggest that, although no GCP-based absolute adjustment was applied, the internal positional consistency of the photogrammetric block was acceptable for local distribution mapping and comparative spatial analysis.

The imagery was processed in Pix4Dmapper Pro version 3.1.23 using the “3D Maps” template. The main processing settings included full-scale keypoint extraction, aerial grid or corridor matching, standard camera calibration, and generation of both DSM and orthomosaic products. Noise filtering and sharp surface smoothing were applied during DSM generation, and the raster DSM was generated using inverse distance weighting interpolation. The orthomosaic output was exported as a merged product for subsequent image interpretation. Because only one archived quality report was available at the time of manuscript revision, the processing details reported here are based on the retained workflow documentation and the authors’ record that the three observation epochs were processed using the same or near-identical procedures.

2.3.2 Image Interpretation and Spatial Delineation

In this study, *M. micrantha* was identified from RGB orthomosaics using visual characteristics associated with its flowering and senescence stages. During the flowering season, *M. micrantha* typically exhibits bright green to whitish-green inflorescences with a fringed texture and a relatively continuous canopy-like appearance. During senescence, the patches become grayish-white to brownish, but remain visually distinguishable from surrounding vegetation in high-resolution aerial imagery. These phenological and textural characteristics, which are summarized in Table 1 and visually presented in Figure 5 and Figure 6, served as the primary interpretation criteria for delineating the species in the orthomosaics.

Manual interpretation was adopted because the target species exhibited recognizable flowering-season features in the high-resolution RGB imagery and because the present study focused on a practical monitoring application based on three limited observation epochs rather than on the development of a fully automated classification model. Delineation was carried out by considering image tone, texture, patch shape, continuity, edge characteristics, and the spatial context of adjacent land cover (Chen et al., 2014b). In addition, *M. micrantha* was commonly found in areas such as agricultural margins, betel nut plantations, grasslands, and forest edges, and these environmental associations also assisted interpretation. After the target patches were identified, their boundaries were manually digitized to produce distribution layers for each observation epoch.

To improve interpretation consistency and reduce personal bias, the delineation process followed four steps: (1) pre-interpretation training, (2) independent delineation by three teams, (3) cross-comparison and revision of the initial outputs, and (4) final review by a senior interpreter. Field photographs and GPS coordinates were also collected and used as reference information during the interpretation process. This workflow was intended to improve the reliability of the final mapped distribution of *M. micrantha* across the three observation epochs. Although this procedure improved the consistency of manual delineation, the interpretation results may still be affected by seasonal phenological variation, illumination conditions, and interpreter judgment. Therefore, the mapped patches were interpreted as management-oriented distribution records rather than fully automated classification outputs.

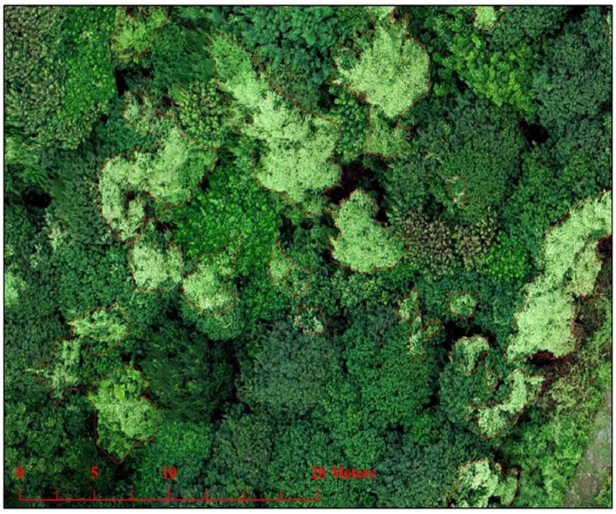

Figure 5. Aerial Imagery of *M. micrantha* During the Flowering Season

Figure 6. Aerial Imagery of *M. micrantha* During the Senescence Phase

https://doi.org/10.5194/isprs-archives-XLIX-B3-2026-121-2026

Classification Criterion	Flowering Season	Senescence Phase
Contour	Irregular	Irregular
Edge	Fringed, ciliate	Ciliate
Surface continuity	Continuous surface	Continuous surface
Size	Variable	Variable
Opacity	Opaque	Semi-transparent
Apex form	Flat, fine-tapered	Flat
Structural depth	Connected canopy, top-layer structure	Connected canopy
Adjacency	Typically connected	More separated
Leaf－branch texture	Smooth	Granular
Hue	Light green, bright green, whitish-green	Dark brown, grayish-black
Chroma (Saturation)	High	Low
Brightness (Value)	High	Low

Table 1. Classification Criteria for UAV Image Interpretation of *M. micrantha* During the Flowering and Senescence Phases

2.3.3 Kernel Density Estimation

To assess the spatial concentration pattern of *M. micrantha*, kernel density estimation (KDE) was applied to the interpreted results from the three observation epochs. KDE was used to transform the interpreted distribution data into continuous density surfaces, thereby highlighting areas with relatively high invasion concentration and facilitating visual comparison of hotspot persistence, reduction, or outward spread among epochs. This approach was used as an exploratory spatial analysis method to reveal the relative distribution intensity of M. micrantha within the monitoring area.

Based on the interpreted distribution maps, the KDE outputs were subsequently classified into six relative density classes to support consistent visual comparison of infestation patterns among the three observation epochs. A common classification scheme was applied across all epochs so that changes in hotspot persistence, peripheral expansion, and newly emerging concentration zones could be compared under the same density thresholds. The six classes used in this study were: Negligible/No Density Zone (0–1,000 m²/km²), Low Density Zone (1,000–50,000 m²/km²), Moderate Density Zone (50,000–70,000 m²/km²), Moderate-High Density Zone (70,000–90,000 m²/km²), High Density Zone (90,000–130,000 m²/km²), and Extreme High Density Zone (>130,000 m²/km²) (Table 2). These classes were used as a relative interpretation framework for map comparison rather than as ecological thresholds of invasion severity.

The resulting density maps were used to identify stable core infestation areas, peripheral expansion zones, and newly emerging hotspots. Because the main purpose of KDE in this study was to support comparative interpretation of local invasion patterns, it was treated as an analytical tool for spatial summarization rather than as a predictive model of invasion dynamics.

2.3.4 Comparison Among Observation Epochs

The final spatial products derived from image interpretation and KDE were compared among three flowering-season observation epochs acquired on 14 January 2021, 7 December 2021, and 4 January 2024. Because these observations were unevenly spaced in time, the analysis was interpreted as a comparison among three observation epochs rather than as a continuous annual time series. For each epoch, the mapped area of *M. micrantha* was calculated and compared, and the KDE surfaces were examined to identify persistent hotspots, short-term reductions, and later re-expansion patterns within the monitoring area. This three-epoch comparison provided the basis for evaluating the spatial persistence and redistribution of *M. micrantha* during the flowering season in the Liyu Lake monitoring region.

3. Results and Discussion

3.1 Changes in the Areal Extent of *M. micrantha*

The distribution of *M. micrantha* was delineated from UAV orthomosaics for three flowering-season observation epochs acquired on 14 January 2021, 7 December 2021, and 4 January 2024. The interpreted infestation area was 2,095 m² for the first epoch, 1,362 m² for the second epoch, and 1,799 m² for the third epoch (Figure 7). Relative to the total monitored area of 34.8746 ha, these values correspond to approximately 0.60%, 0.39%, and 0.52% of the study area, respectively. Overall, the mapped extent showed a decline between the first and second epochs, followed by a re-expansion by the third epoch.

The decrease from the first to the second epoch should not be interpreted simply as a sustained decline in invasion severity. Instead, it more likely reflects a short-term reduction in visible flowering-season coverage within the monitored area. Because *M. micrantha* is capable of rapid vegetative regeneration and reinvasion from stem fragments and seed sources, a temporary reduction in mapped area does not necessarily indicate long-term suppression. The increase observed in the third epoch suggests that the species remained active in the landscape and was able to re-establish after the earlier decline. This pattern is consistent with the strong regenerative capacity of *M. micrantha* described in the study background and supports the need for repeated monitoring rather than one-time assessment.

It is also important to note that the three observations were not evenly spaced in time and were not acquired on the same calendar date within the flowering season. The interval between the first and second epochs was approximately 11 months, whereas the interval between the second and third epochs was approximately 25 months. In addition, the second epoch was acquired several weeks earlier in the flowering season than the first and third epochs. Therefore, the area differences reported here should be interpreted as comparisons among three unevenly spaced observation epochs rather than as a continuous annual time series. Differences in flowering expression and phenological timing may have influenced the visual detectability of *M. micrantha* in the RGB orthomosaics, especially when manual interpretation was based on flowering- and senescence-related image characteristics.

Taken together, the areal results indicate that *M. micrantha* remained persistently established in the monitoring area throughout the observation period. Although the total mapped extent fluctuated, the species did not disappear from the site, and the third epoch confirmed renewed expansion following the earlier reduction. From a management perspective, this suggests that local suppression, even if temporarily effective, may not be sufficient to prevent re-establishment without continued follow-up and spatially targeted intervention.

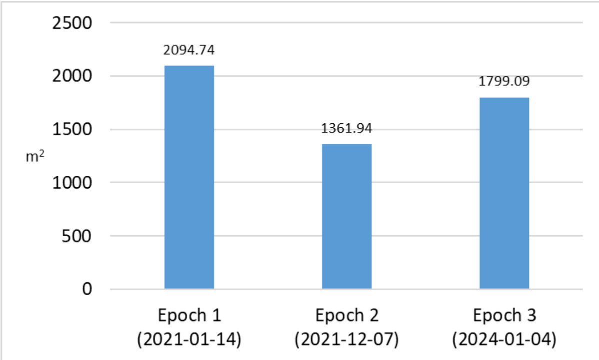

Figure 7. Interpreted Areal Extent of *M. micrantha* Across the Three Observation Epochs

3.2 Changes in the Spatial Distribution of *M. micrantha*

The comparison of distribution maps among the three observation epochs revealed both spatial persistence and redistribution of *M. micrantha* within the monitoring area (Figures 8 and 9). In the first epoch, the mapped patches were relatively scattered but already concentrated around several local core zones. In the second epoch, although the total interpreted area decreased, the distribution pattern suggested that the remaining patches were still associated with the original core area and nearby surroundings. By the third epoch, the mapped distribution became more extensive again, and several patches appeared to spread outward from previously occupied locations, indicating continued persistence and renewed local expansion.

This spatial pattern suggests that the invasion did not follow a simple “expansion-only” trajectory. Instead, the observed changes are more consistent with contraction and re-expansion around persistent source areas. In other words, some portions of the infestation may have been temporarily reduced or become less visually apparent during the second observation epoch, but the overall spatial framework of the invasion remained present in the landscape. Such a pattern is ecologically plausible for *M. micrantha*, which can persist through residual propagules or vegetative fragments and subsequently reoccupy nearby habitat when environmental conditions become favorable.

The overlaid distribution map further indicates that the core invaded zone remained broadly stable among epochs, while the peripheral patches changed more noticeably. This is an important management signal. Stable recurrence in the same central locations suggests that these areas may function as persistent infestation reservoirs, whereas the changing peripheral patches may represent short-distance spread fronts or reinvasion from remnant individuals. Accordingly, future control strategies should not focus only on total area reduction, but should also prioritize repeated treatment and inspection of stable core zones that are likely to act as continuing sources of spread.

Because the present study relied on manual interpretation of RGB orthomosaics, the mapped distribution should also be understood in relation to the species’ visible flowering-season characteristics. The observed spatial differences among epochs likely reflect a combination of actual infestation change and variation in seasonal expression. Nevertheless, the recurrence of similar core locations and the reappearance of expanded patches in the third epoch indicate that the overall invasion pattern was not random and that UAV-based image interpretation was able to capture meaningful local distribution dynamics.

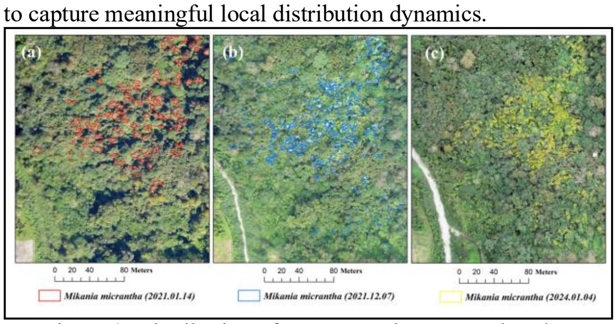

Figure 8. Distribution of *M. micrantha* Across the Three Observation Epochs
(a) 14 January 2021
(b) 7 December 2021
(c) 4 January 2024

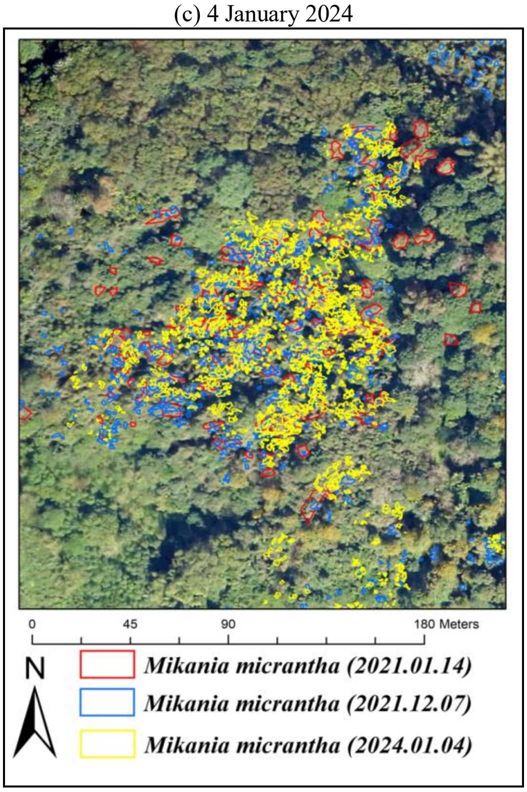

Figure 9. Overlaid Distribution Map of *M. micrantha* Across the Three Observation Epochs

3.3 Changes in the Density and Spreading Patterns of *M. micrantha*

Kernel density estimation (KDE) was used to summarize the relative spatial concentration of *M. micrantha* across the three observation epochs. To ensure comparability, all KDE maps were visualized using the same six density classes shown in Table 2. The mean kernel density declined from 37,001.43 m^2/km^2 in the first epoch to 24,595.93 m^2/km^2 in the second epoch, before increasing to 32,557.09 m^2/km^2 in the third epoch (Figure 10). This pattern generally corresponded to the change in interpreted infestation area and suggests a temporary weakening followed by renewed concentration of infestation within the monitored area.

However, the KDE results provide additional information beyond simple area statistics. While total mapped area describes the overall extent of visible infestation, kernel density emphasizes how strongly the infestation is concentrated in space. The decrease in mean density during the second epoch suggests not only reduced mapped area but also a weakening of the overall concentration of infestation within the monitored landscape. Conversely, the increase in the third epoch indicates that *M. micrantha* did not merely reappear as isolated small patches, but regained a more spatially consolidated presence. This distinction is important because increases in density may imply a higher likelihood of local persistence, vegetative dominance, and future spread pressure from established source zones.

The kernel density maps (Figure 11) further showed that the infestation pattern changed unevenly across density classes. In the first epoch, high-density and extreme high-density zones were concentrated within several core outbreak areas. In the second epoch, low-density areas expanded outward more clearly, suggesting a broader but less concentrated spatial signal. By the third epoch, the high-density core zones remained generally similar in location, while moderate-density areas became more evident in the southeastern part of the monitoring area, indicating the emergence of a new potential hotspot. This pattern suggests that the invasion was characterized by both persistence of established core areas and progressive reorganization along the margins of the monitored area.

From an ecological and management perspective, the KDE results imply that *M. micrantha* in this site had already developed a partially stabilized invasion structure: central source areas remained active, while lower-density and moderate-density patches shifted around them and expanded into adjacent space. Such a pattern is particularly relevant for control planning because it indicates that management should simultaneously address two spatial components: long-term suppression of persistent core infestation zones and early intervention in newly developing peripheral hotspots. If only the visible dense patches are removed, lower-density surrounding areas may continue to serve as pathways for reinvasion and later re-concentration.

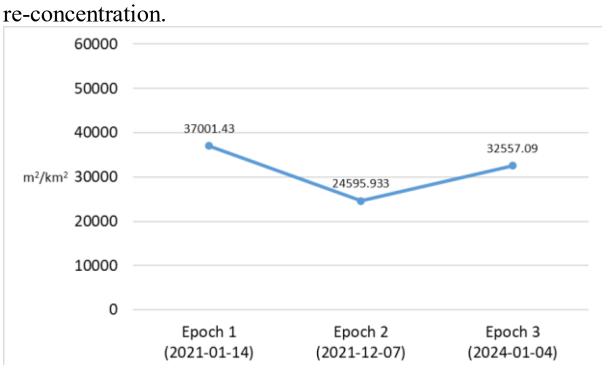

Figure 10. Mean Kernel Density of *M. micrantha* Across the Three Observation Epochs

Table 2. Common kernel density classification scheme used to compare the relative infestation intensity of *M. micrantha* across the three observation epochs.

Classification	Density range (m^2/km^2)
Negligible/No Density Zone	0-1,000
Low Density Zone	1,000-50,000
Moderate Density Zone	50,000-70,000
Moderate-High Density Zone	70,000-90,000
High Density Zone	90,000-130,000
Extreme High Density Zone	Over 130,000

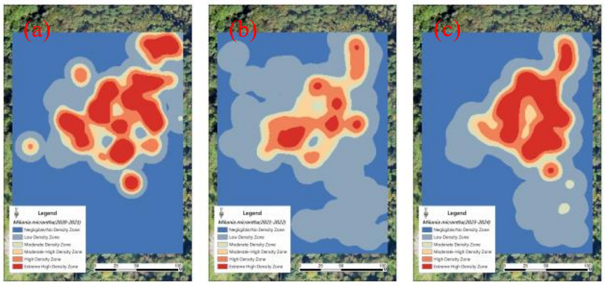

Figure 11. Changes in the Kernel Density Distribution of M. micrantha Across the Three Observation Epochs
(a) 14 January 2021
(b) 7 December 2021
(c) 4 January 2024

4. Conclusion

Taken together, the area-based and density-based analyses indicate that *M. micrantha* in the monitored area did not undergo a simple monotonic increase or decrease. Instead, the results support a pattern of temporary decline followed by renewed expansion, with persistent central infestation zones and changing peripheral spread. This interpretation is more consistent with the biology of the species and with the uneven observation design than a strictly linear temporal trend. The three UAV surveys should therefore be regarded as multi-epoch snapshots of flowering-season distribution rather than as a continuous time-series record.

This distinction is important when interpreting the apparent reduction in the second epoch. Because the second survey was conducted earlier in the flowering season than the first and third surveys, part of the observed difference may have been influenced by phenological timing in addition to actual infestation change. Therefore, the lower mapped area and lower mean density in the second epoch should be interpreted cautiously. Even so, the recurrence of hotspot locations and the renewed expansion observed in the third epoch strongly suggest that *M. micrantha* maintained a persistent foothold in the monitored landscape and was capable of rapid local re-establishment.

Despite the limited number of observation epochs, the UAV-based workflow still demonstrated clear practical value. The orthomosaics provided sufficiently fine spatial detail for identifying flowering-season patches of *M. micrantha*, while the combination of manual delineation and KDE supported interpretation of both visible extent and concentration patterns. In management terms, the results show that repeated UAV monitoring can help distinguish stable source zones from transient peripheral spread, thereby improving the spatial prioritization of follow-up control. This is especially useful in heterogeneous lowland landscapes where invasion fronts may shift quickly and where field-only surveys are comparatively time-consuming.

At the same time, the present results should be interpreted within the limitations of the study. Only three observation epochs were available, the intervals between observations were unequal, and the analysis was based on RGB image interpretation rather than automated multispectral or machine-learning classification. Accordingly, the present study is best understood as a practical multi-epoch monitoring case study rather than a full temporal modeling analysis. Even with these limitations, the results still provide useful spatial evidence of persistence, redistribution, and reinvasion risk, and they establish a baseline for future work incorporating more frequent surveys, improved seasonal standardization, and automated extraction methods.

Acknowledgements

The authors would like to express their sincere gratitude to all individuals and organizations who supported the implementation and completion of this study. We thank all colleagues and collaborators who contributed to UAV image acquisition, data processing, field investigation, and technical discussion during the course of this research. Their valuable assistance and professional insights greatly contributed to the successful completion of this work. We also acknowledge the support provided by the relevant institutions in facilitating access to the study area, data collection, and field operations, which improved both the efficiency and quality of this research. Finally, the authors sincerely appreciate the valuable comments and suggestions provided by the reviewers, which helped improve the content and overall quality of this manuscript.

References

Chen, C.C., Huang, S.C., Chen, Y.K., Teng, K.C., Chen, C.Z., 2014b. Establishment and application of aerial photo interpretation indices for major broadleaf tree species in Taiwan. Quarterly Journal of Chinese Forestry 47(4), 399-426.

Chen, C.Z., 2017. Ecological benefits assessment of Leucaena removal and restoration. Technical Report 104-6-5-01, Pingtung Branch, Forestry and Natural Conservation Agency, Council of Agriculture, Executive Yuan, 158 pp.

Feng, L., Chen, S., Zhang, C., Zhang, Y., He, Y., 2021. A comprehensive review on recent applications of unmanned aerial vehicle remote sensing with various sensors for high-throughput plant phenotyping. Computers and Electronics in Agriculture 182: 106033.

Huang, S.Y., Peng, J.J., Guo, Y.H., 2003. Spread and monitoring of *Mikania micrantha* in Taiwan. Proceedings of the Symposium on the Impacts and Management of *Mikania micrantha* 1, 123-145.

Meiners, S.J., Pickett, S.T.A., Cadenasso, M.L., 2001. Effects of plant invasions on the species richness of abandoned agricultural land. Ecography 25: 215-223.

Nyamekye, C., Ghansah, B., Agyapong, E., Obuobie, E., Awuah, A., Kwofie, S., 2021. Examining the performances of true color RGB bands from Landsat-8, Sentinel-2 and UAV as stand-alone data for mapping artisanal and small-scale mining (ASM). Remote Sensing Applications: Society and Environment 24, 100655.

Pyšek, P., Richardson, D.M., Rejmánek, M., Webster, G.L., Williamson, M., Kirschner, J., 2004. Alien plants in checklists and floras: towards better communication between taxonomists and ecologists. Taxon 53: 131-143.

Seebens, H., Blackburn, T.M., Dyer, E.E., Genovesi, P., Hulme, P.E., Jeschke, J.M., Pagad, S., Pyšek, P., van Kleunen, M., Winter, M., Ansong, M., Arianoutsou, M., Bacher, S., Blasius, B., Brockerhoff, E.G., Brundu, G., Capinha, C., Causton, C.E., Celesti-Grapow, L., Dawson, W., Dullinger, S., Economo, E.P., Fuentes, N., Guénard, B., Jäger, H., Kartesz, J., Kenis, M., Kühn, I., Lenzner, B., Liebhold, A.M., Mosena, A., Moser, D., Nentwig, W., Nishino, M., Pearman, D., Pergl, J., Rabitsch, W., Rojas-Sandoval, J., Roques, A., Rorke, S., Rossinelli, S., Roy, H.E., Scalera, R., Schindler, S., Stajerová, K., Tokarska-Guzik, B., Walker, K., Ward, D.F., Yamanaka, T., Essl, F., 2018. Global rise in emerging alien species results from increased accessibility of new source pools. Proceedings of the National Academy of Sciences of the United States of America 115(10): 2264-2273.

Tian, K.G., Tsai, C.H., Lin, K.F., 2017. Application of UAV and laser scanning technology for volumetric assessment of gravel stockpiles. Journal of Photogrammetry and Remote Sensing 22(2), 127-136.

Tye, A., 2006. Can we infer island introduction and naturalization rates from inventory data? Evidence from introduced plants in Galapagos. Biological Invasions 8: 201-215.

Wei, Z.Y., 2003. Spatial distribution of *Mikania micrantha* invasion analyzed using GIS. Master's thesis, Department of Forestry, National Pingtung University of Science and Technology, 79 pp.